The Binary Singularity Model

A Physical Hypothesis for Sub-Planckian Lattice Structure and Fundamental Constants

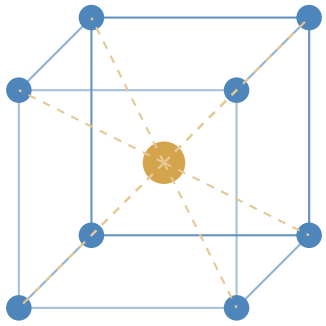

$n = 8$ *nearest neighbors*

Alan Garcia

Independent Researcher

alan.javier.garcia@gmail.com

February 2026

"What would have to be true for a photon to behave as both a wave and a particle?"

This document summarizes the physical hypothesis underlying the Binary Singularity Model (BSM): a framework in which fundamental constants emerge from the spectral geometry of a body-centered cubic lattice. Two inputs—the BCC coordination number $n = 8$ and the transcendental π—with spatial dimension $d = 3$ entering higher-order formulas, produce six fundamental constants with zero free parameters.

Contents

1 Origin: The Photon as a Composite Object

Core Hypothesis

The photon is a composite of two sub-Planck-scale singularities in helical orbit. Viewed from the side, the orbit traces a wave; viewed head-on, it appears as a point. Wave–particle duality emerges from the geometry of the binary orbit.

The Binary Singularity Model began with a question about wave–particle duality: what physical structure could produce both wave-like and particle-like behavior from the same object? The proposed answer is a binary system of two gravitational singularities orbiting each other at a scale far below the Planck length ($\ell_P \approx 1.6 \times 10^{-35}$ m). At such scales, the concept of "probing with light" breaks down—wavelengths short enough to resolve the structure would carry enough energy to collapse into black holes—making the sub-Planckian regime causally inaccessible to direct measurement.

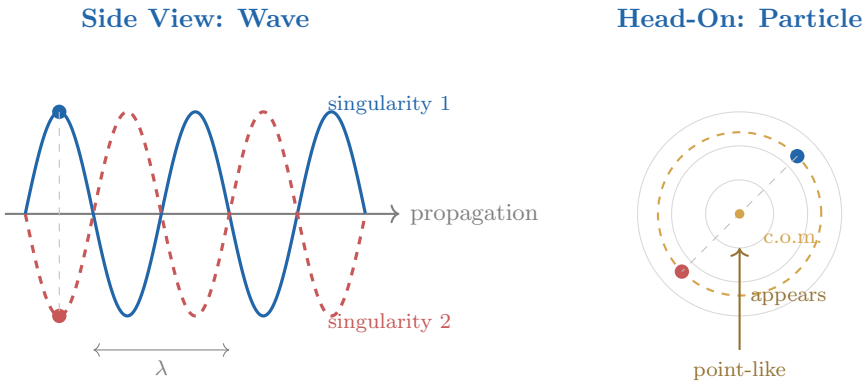

Figure 1: The binary singularity hypothesis. Two sub-Planckian singularities in helical orbit appear as a wave (side view) or a particle (head-on). The wavelength λ and energy $E = hc/\lambda$ are determined by the orbital parameters.

The self-consistency requirement—that such a binary system respect both quantum mechanics and general relativity at its own scale—forces structural constraints. Over iterative computation, these constraints converged on a body-centered cubic (BCC) lattice as the underlying spatial geometry. The BSM framework then identifies all particles as topological defects on this lattice, and the photon as the longitudinal propagation mode of the binary defect.

2 The BCC Lattice

The body-centered cubic lattice is defined by corner sites plus a central site in each cubic unit cell. Each site has $n = 8$ nearest neighbors (coordination number). This is the fundamental input of the BSM framework.

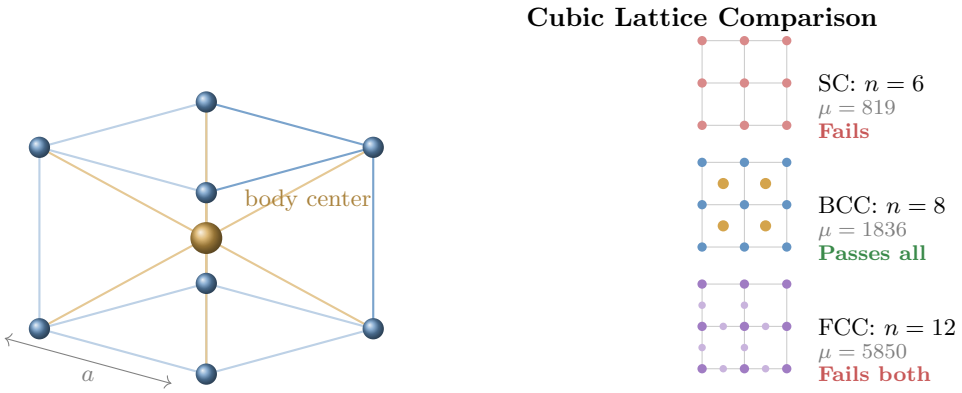

Figure 2: **Left:** The BCC unit cell. Eight corner sites (blue) each share 1/8 with adjacent cells; the body-center site (gold) belongs entirely to this cell. Each site has $n = 8$ nearest neighbors. **Right:** Only BCC ($n = 8$) yields the correct mass generator $\mu = 1836 \approx m_p/m_e$.

2.1 Why BCC?

The tree-level proton–electron mass generator $\mu(n) = \frac{3}{2}\sigma(n) \cdot \rho(n)$ uniquely selects BCC. Simple cubic ($n = 6$) gives $\mu = 819$, which is 55% below the experimental proton mass ratio. FCC ($n = 12$) gives $\mu = 5850$, which is 219% too high. No perturbative correction can bridge these gaps. The BCC lattice is the *only* cubic lattice whose coordination number yields both $\tau(8) = 137$ and $\mu(8) = 1836$.

3 Generator Functions from SO(3) Representation Theory

Four generator functions of the coordination number n, arising from the representation theory of SO(3), build all observable quantities:

The Four Generators

$$\tau(n) = n(2n+1) + 1 \quad \text{(topological: } \dim \Lambda^2 D(n) \oplus D(0)\text{)} \tag{1}$$

$$\sigma(n) = n(2n+1) \quad \text{(pairwise: } \tbinom{2n+1}{2} \text{ substate couplings)} \tag{2}$$

$$\rho(n) = n + 1 \quad \text{(radial: shells in spin-}n\text{ representation)} \tag{3}$$

$$\mu(n) = \tfrac{3}{2}\,\sigma(n)\,\rho(n) \quad \text{(mass: composite generator)} \tag{4}$$

At $n = 8$: $\tau = 137$, $\sigma = 136$, $\rho = 9$, $\mu = 1836$.

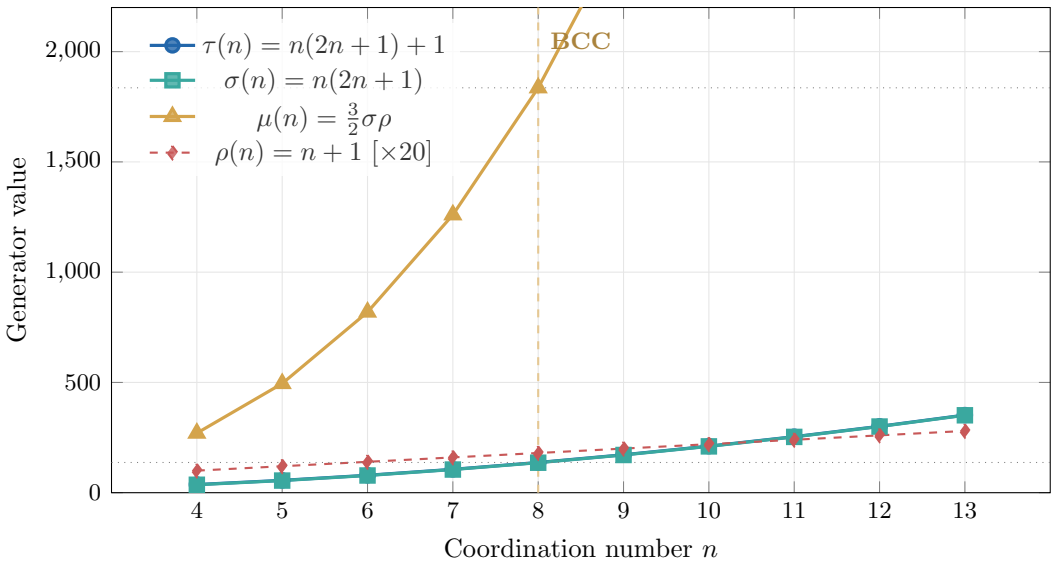

Figure 3: The four BSM generator functions versus coordination number n. At $n = 8$ (BCC, dashed gold line), $\tau = 137 \approx \alpha^{-1}$ and $\mu = 1836 \approx m_p/m_e$. The horizontal dotted lines mark the experimental values.

4 Particles as Lattice Defects

In the BSM framework, every particle is a topological defect—a localized disturbance in the BCC lattice. The defect classification determines the particle spectrum.

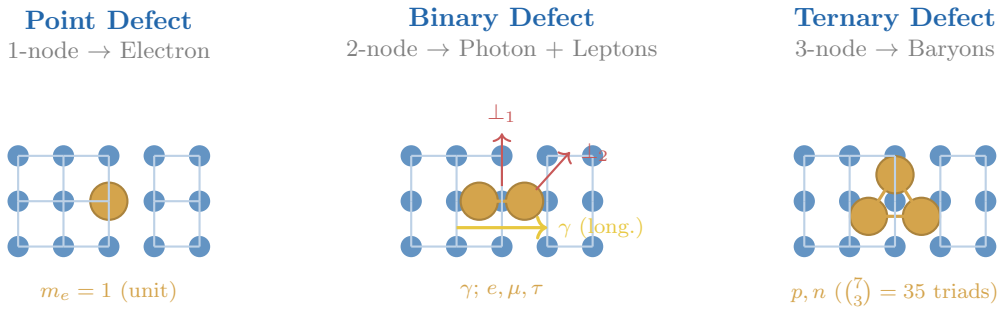

Figure 4: The BSM defect classification. The **binary defect** (2-node line) hosts the photon as its longitudinal mode (yellow arrow) and the three lepton generations as transverse excitations (red arrows). The **ternary defect** (3-node triangle) embeds in $\binom{n-1}{d} = 35$ orientational triads.

5 The Photon on the BCC Lattice

The photon is the best-characterized object in the BSM framework: its dressed propagator yields $\alpha^{-1} = 137.035\,999\,177$, matching CODATA to < 0.001 ppb. This section consolidates the photon's geometric identity, field-theoretic interpretation, dispersion relation, and observational constraints.

5.1 Geometric Identity: Longitudinal Mode of the Binary Defect

A bond in d dimensions decomposes into:

- 1 longitudinal direction (along the bond) $\longrightarrow$ **photon**
- $d-1=2$ transverse directions (normal to the bond) $\longrightarrow$ **charged leptons** (e,μ,τ)

The Koide parameter $Q=(d-1)/d=2/3$ counts the transverse fraction. The photon occupies the remaining $1/d$ fraction.

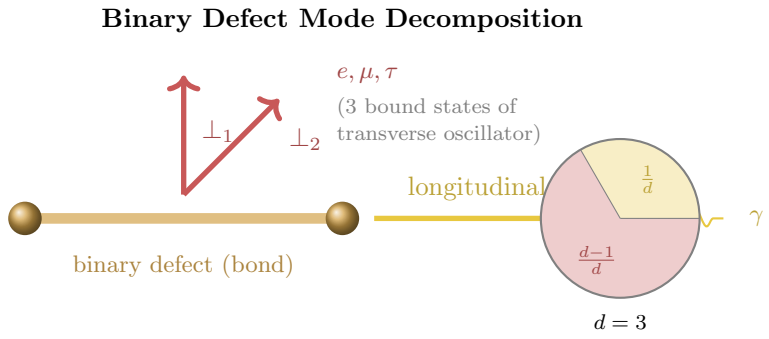

The photon is the U(1) gauge mode: a phase variable $e^{i\theta}$ on each bond. Curvature (field strength $F_{\mu\nu}$) lives on plaquettes—the smallest closed loops of the BCC lattice.

Figure 5: The binary defect decomposes into a longitudinal mode (the photon, $1/d$ of degrees of freedom) and transverse modes (the leptons, $(d-1)/d$ of degrees of freedom). In $d=3$: 1 photon direction, 2 transverse directions hosting 3 lepton generations.

5.2 The Dyson Equation as the Photon's Self-Energy

The BSM formula for α^{-1} is interpreted as a dressed photon propagator:

$$\boxed{\alpha^{-1}=B+\frac{1}{(n{+}2)\,B^2}}, \qquad B=\tau+\frac{c_1}{\tau}-\frac{1}{2\tau^2}-\frac{1}{(n{-}1)\tau^3}+\frac{c_4}{\tau^4} \tag{5}$$

with $c_1=\pi^2/2$ (Brillouin zone integral), $c_4=\frac{18}{17}\pi^3$ (spectral skewness). The lattice parameters are coupling $g^2=1/2$ and Dirac multiplicity $N_D=4$. This has the structure of a Dyson equation $G^{-1}=G_0^{-1}-\Sigma(G)$, where the loop coefficients encode the BCC geometry as seen by the photon.

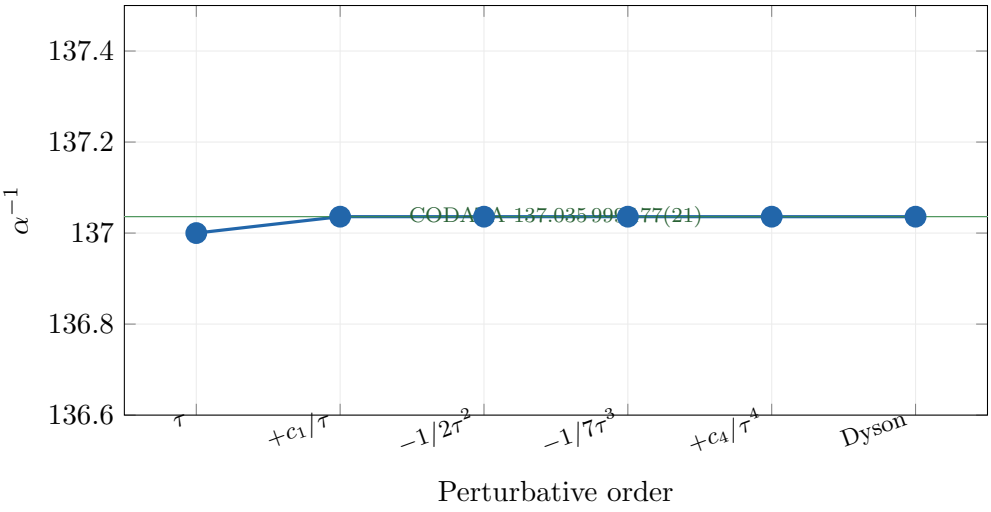

Figure 6: Convergence of α^{-1} as successive perturbative corrections are added. The tree level $\tau = 137$ is corrected order-by-order; the final Dyson resummation yields agreement with CODATA to < 0.001 ppb.

5.3 Complex Structure of the Dyson Cubic

The Dyson equation is a cubic $z^3 - Bz^2 - 1/(n{+}2) = 0$ with discriminant $\Delta < 0$: one real root $z_1 = \alpha^{-1}$ and a complex conjugate pair $z_{2,3} \approx \pm 0.027\, i$. By Vieta's formulas, $|z_{2,3}|^2 = \alpha/(n+2)$, so the complex roots have modulus $\sim \sqrt{\alpha}$. The physical coupling is separated from the complex pair by $\alpha^{-1}/|z_2| \approx 5000$.

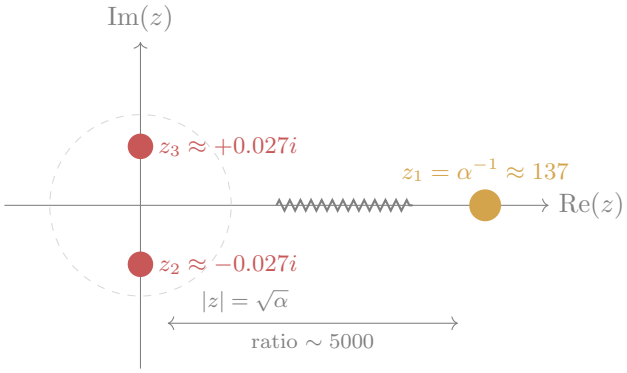

Figure 7: Complex roots of the BSM Dyson cubic. The physical root $\alpha^{-1} \approx 137$ lies far from the complex pair $|z_{2,3}| \sim \sqrt{\alpha}$, confirming deep perturbative stability.

5.4 Lattice Dispersion Relation

On any lattice with spacing a, the photon dispersion relation in the tight-binding approximation is:

$$\boxed{\omega(k) = \frac{2c}{a}\left|\sin\left(\frac{ka}{2}\right)\right|} \tag{6}$$

At long wavelengths ($ka \ll 1$), this recovers $\omega = ck$ with corrections of order $(ka)^2$. The group velocity is $v_g = c\cos(ka/2) = c[1 - (ka)^2/8 + \cdots]$.

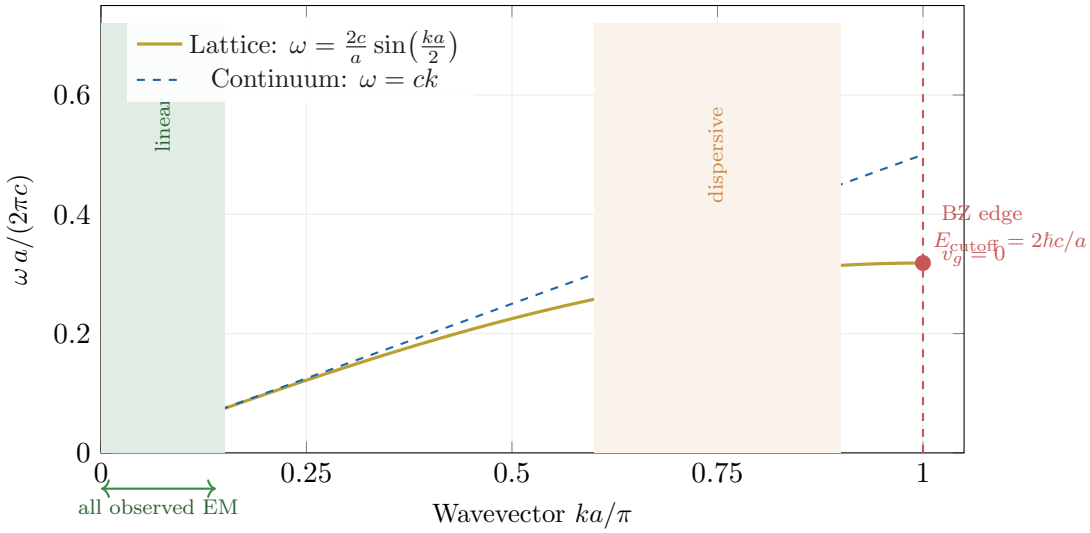

Figure 8: The lattice dispersion relation $\omega(k)$ (solid gold) versus the continuum linear relation $\omega = ck$ (dashed blue). Three regimes emerge: a linear regime ($ka \ll 1$, indistinguishable from continuum), a dispersive regime ($ka \sim 1$, $v_g < c$), and the Brillouin zone edge ($k = \pi/a$, standing wave, $v_g = 0$). *All observed electromagnetic radiation* occupies the green band at the far left.

5.5 Group Velocity and Vacuum Dispersion

The lattice predicts a phenomenon absent from continuum QED: *vacuum dispersion*. High-energy photons travel slightly slower than low-energy ones:

$$\frac{\Delta v}{c} = 1 - \cos\left(\frac{ka}{2}\right) \approx \frac{1}{2}\left(\frac{Ea}{4\pi\hbar c}\right)^2 \tag{7}$$

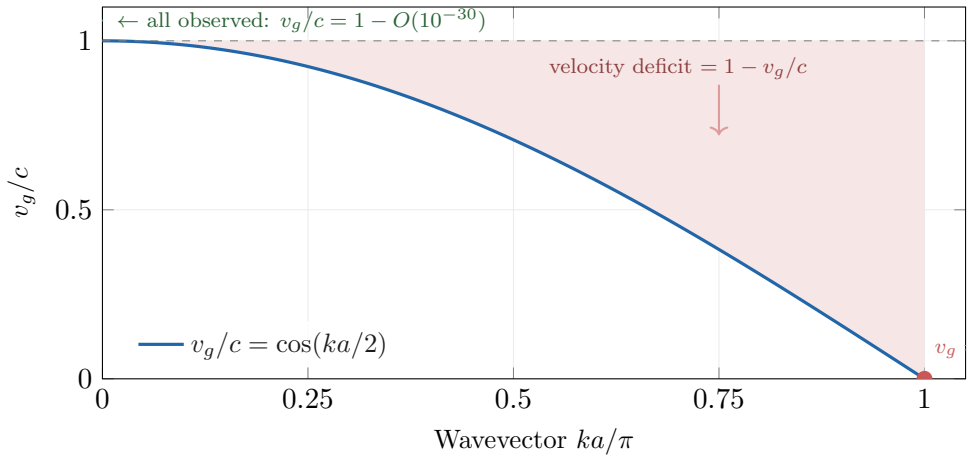

Figure 9: Group velocity $v_g/c = \cos(ka/2)$ on the lattice. The shaded area shows the velocity deficit. At the Brillouin zone edge, $v_g \to 0$ and the photon becomes a standing wave. For all observed electromagnetic radiation, the deviation from c is below 10^{-30}—far beyond any conceivable measurement.

5.6 The Electromagnetic Spectrum on the Lattice

The lattice becomes visible only at trans-Planckian energies. Assuming the natural sub-Planckian spacing $a = \ell_P/\tau \approx 1.18 \times 10^{-37}$ m:

Radiation	**Energy**	$ka/2$	**Dispersion**	$1 - v_g/c$
Radio (FM)	$\sim 10^{-7}$ eV	$\sim 10^{-37}$	none	$< 10^{-73}$
Green light	2.33 eV	$\sim 10^{-31}$	none	$< 10^{-61}$
Hard X-ray	100 keV	$\sim 10^{-26}$	none	$< 10^{-51}$
Gamma (1 MeV)	10^{6} eV	$\sim 10^{-25}$	none	$< 10^{-49}$
Gamma (1 TeV)	10^{12} eV	$\sim 10^{-19}$	none	$< 10^{-37}$
Gamma (100 TeV)	10^{14} eV	$\sim 10^{-17}$	none	$< 10^{-33}$
Planck energy	1.22×10^{28} eV	3.6×10^{-3}	~ 2 ppm	6.7×10^{-6}
Cutoff	$\sim 3.3 \times 10^{30}$ eV	$\pi/2$	standing wave	$v_g = 0$

Table 1: The electromagnetic spectrum on the BCC lattice. For every photon ever observed—from radio to the highest cosmic gamma rays—the lattice deviation is identically zero to any measurable precision.

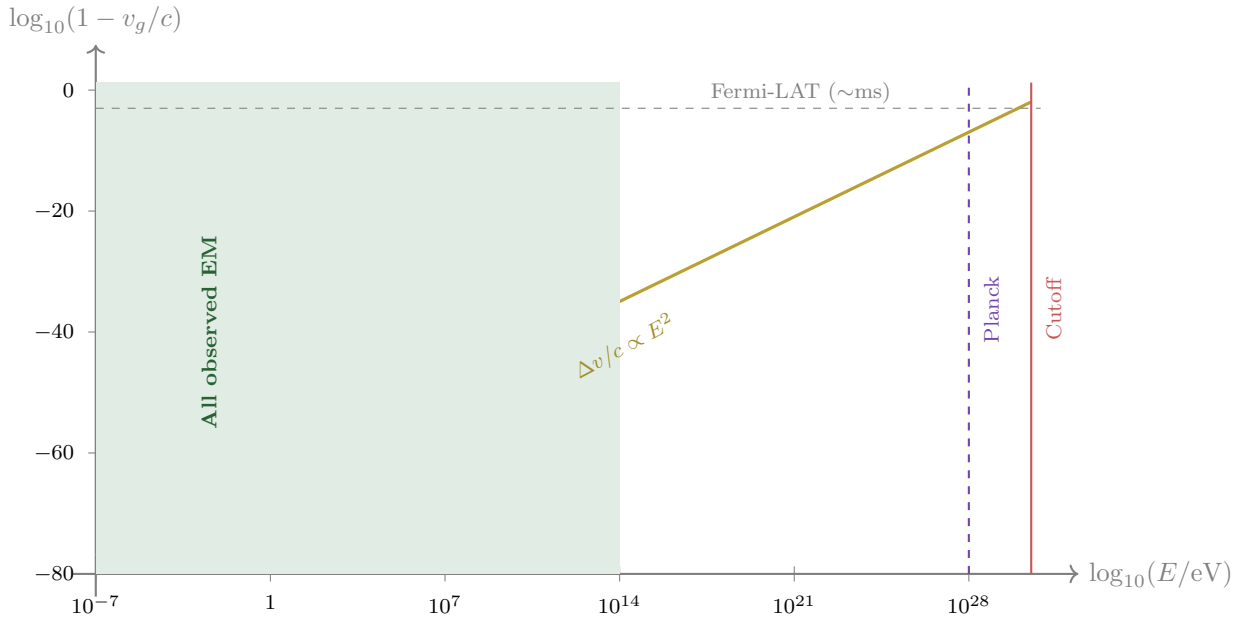

Figure 10: Vacuum dispersion $1 - v_g/c$ versus photon energy (log-log). The relation is quadratic: $\Delta v/c \propto E^2$. All observed electromagnetic radiation (green shaded region) produces deviations far below any conceivable measurement sensitivity. The lattice becomes visible only near the Planck energy (purple dashed line) and reaches complete standing-wave cutoff (red solid line) at $E_{\text{cutoff}} = 2\hbar c/a$.

5.7 Observational Constraints on the Lattice Spacing

The Fermi-LAT constrains vacuum dispersion using arrival-time differences of gamma-ray photons from distant sources. For the quadratic dispersion that a lattice produces, the constraint is $E_{\text{QG}} \gtrsim$

1.3×10^{20} eV, translating to $a \lesssim 3 \times 10^{-30}$ m $\approx 2 \times 10^{5}\,\ell_P$. A sub-Planckian lattice ($a \ll \ell_P$) is safely consistent.

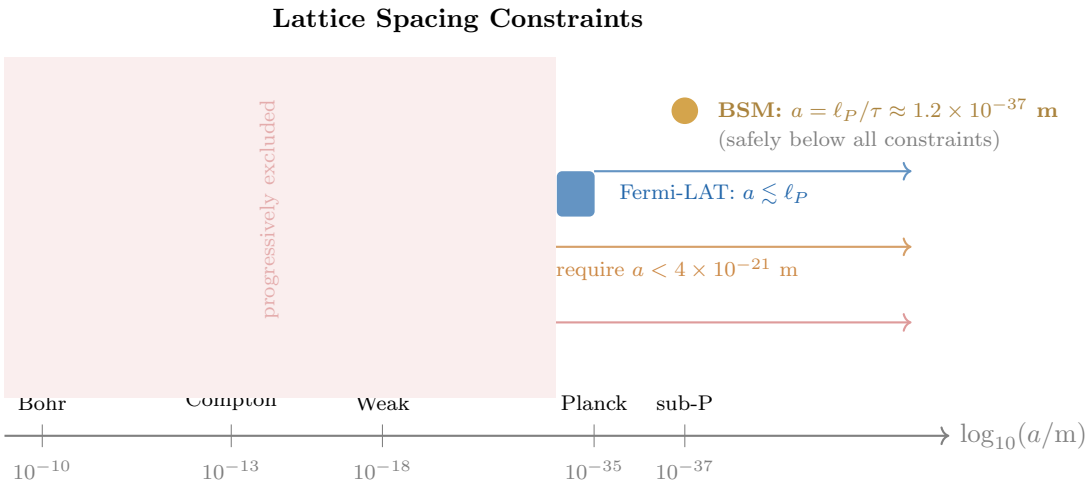

Figure 11: Observational constraints on the lattice spacing a. Each constraint eliminates lattice spacings above its threshold. The BSM natural scale $a = \ell_P/\tau$ (gold dot) lies far below all observational bounds.

5.8 Optical Phenomena from the Lattice

The lattice accounts for all familiar photon properties:

Photon Properties from the BCC Lattice

Masslessness The photon is a gauge mode: the U(1) phase along a bond is a flat direction of the lattice action, protected by gauge invariance. $\omega(0) = 0$.

Polarization A bond oriented along $\hat{x}$ supports transverse fluctuations in $\hat{y}$ and $\hat{z}$: $d - 1 = 2$ polarization states. The longitudinal mode is pure gauge.

Speed of light $c = \lim_{k\to 0} \omega/k$ is the lattice propagation velocity, determined by bond stiffness over inertia per site. Not an external input.

Bose statistics The binary defect has $\mathbb{Z}_2$ symmetry (node exchange). The longitudinal mode is symmetric $\Rightarrow$ Bose–Einstein statistics. Transverse modes are antisymmetric $\Rightarrow$ Fermi–Dirac (leptons).

Refraction On the bare lattice, $n_{\text{refr}} = 1$ exactly. Defects (matter) produce forward scattering with amplitude $\propto \alpha$, shifting the effective phase velocity: $n_{\text{refr}} = 1 + (\text{density}) \times f(\omega)$.

Diffraction Native to lattice waves. The photon diffracts identically to continuum waves for $\lambda \gg a$.

Wave–particle duality **Wave:** delocalized lattice mode obeying $\omega(k)$. **Particle:** interaction with localized defects at specific sites. "Collapse" = lattice wave exciting a localized defect.

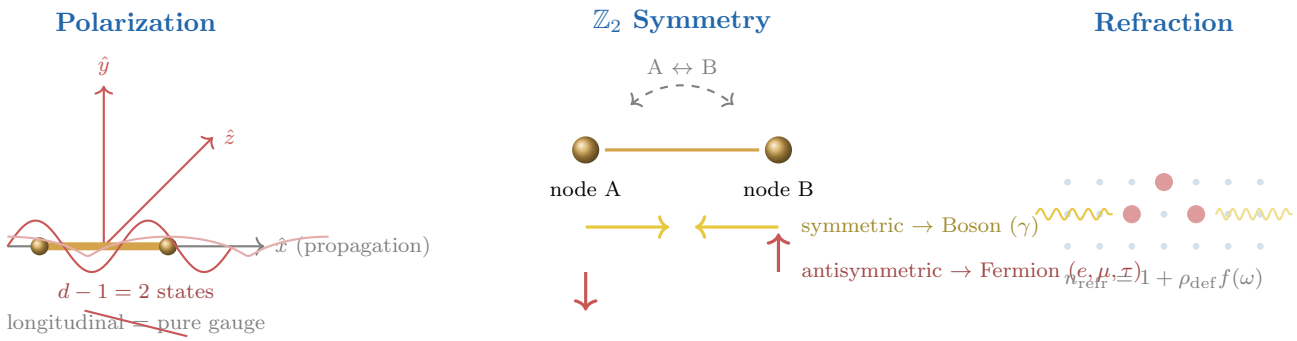

Figure 12: Optical phenomena on the lattice. **Left:** Polarization arises from $d-1=2$ transverse oscillation directions; the longitudinal mode is eliminated by gauge invariance. **Center:** The $\mathbb{Z}_2$ node-exchange symmetry gives Bose statistics to the symmetric (photon) mode and Fermi statistics to the antisymmetric (lepton) modes. **Right:** Refraction arises from forward scattering off lattice defects (matter) with amplitude $\propto \alpha$.

5.9 The Photon–Higgs Connection

The Higgs boson is the breathing mode of the lattice: uniform oscillation of spacing $a(t) = a_{\text{BCC}}[1 + h(t)]$, where $h(t)$ is the Higgs field. The photon propagates *on* this oscillating lattice, making the two modes fundamentally coupled.

If the lattice spacing oscillates, the photon dispersion becomes time-dependent: $\omega(k,t) \approx ck[1 - h(t)]$. This is parametric phase modulation—the same mechanism as Brillouin scattering in condensed matter. The modulation depth per site is α/ρ; integrated over the BZ gives $\pi\alpha/\rho = 0.002547$, which is *exactly* the Higgs VP correction factor.

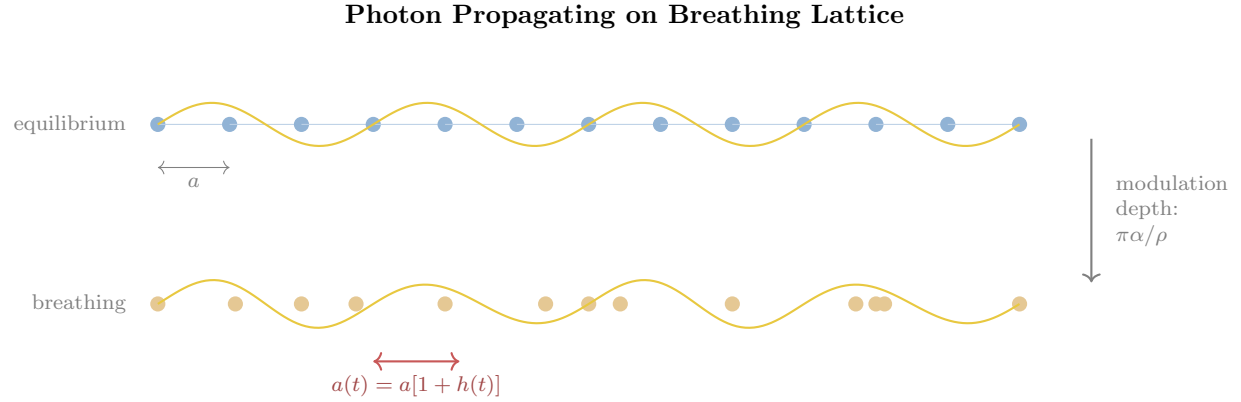

Figure 13: The photon–Higgs coupling. **Top:** Photon propagating on a static lattice (equilibrium spacing a). **Bottom:** The same photon on a breathing lattice ($a(t) = a[1 + h(t)]$). The amplitude modulation is the physical origin of the Higgs VP correction $\pi\alpha/\rho$. This coupling is intrinsically quantum—it turns on at one loop through the BZ integral $c_1 = \pi^2/2$.

Photon's Channel in the Higgs Mass

The Standard Model has $d+1=4$ gauge bosons (W^+, W^-, Z, γ). Three become massive; the photon stays massless because $\mathrm{U}(1)_{\mathrm{EM}}$ is unbroken. In BSM, the Goldstone subtraction removes $d=3$ modes (not $d+1$). The photon's masslessness *raises* the Higgs mass by exactly one dressed proton mass:

$$m_H^{\gamma\,\text{massless}} - m_H^{\gamma\,\text{massive}} = \left(1+\frac{\pi\alpha}{\rho}\right) m_p \approx 940.7\ \text{MeV}$$

The photon contributes one scalar channel to the Higgs sector precisely because $\mathrm{U}(1)_{\mathrm{EM}}$ is unbroken.

6 The Four-Channel Correction Taxonomy

Every BSM formula shares a universal four-channel correction structure.

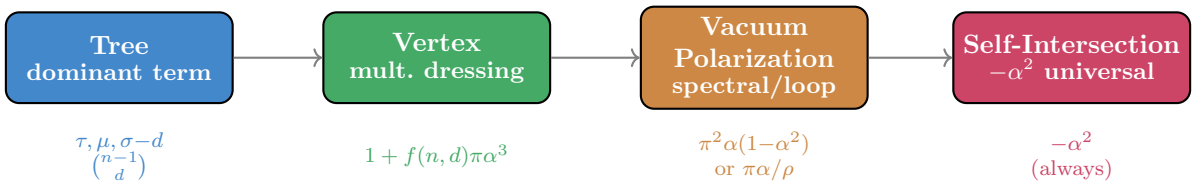

Figure 14: The universal four-channel correction taxonomy.

Observable	Tree	Vertex	VP	Self-int.
α^{-1}	$\tau = 137$	$c_1/\tau, \ldots, c_4/\tau^4$	$1/(n{+}2)B^2$	(Dyson)
m_p/m_e	$\mu = 1836$	$\times(1{+}2(2n{+}1)\pi\alpha^3)$	$(1{+}\frac{1}{2n})\pi^2\alpha(1{-}\alpha^2)$	$-\alpha^2$
m_μ/m_e	$\frac{d}{2}\tau = 205.5$	$+\frac{d}{2}\pi\sigma\alpha^3$	$\frac{d}{2}\pi\alpha(1{-}\alpha^2)$	$-\alpha^2$
m_τ/m_e	Koide: $Q = \frac{d-1}{d}$	$\delta Q = \frac{(d-1)\pi^2\alpha^2}{(n-1)\sigma}$		—
m_H/m_p	$\sigma - d = 133$	—	$\times(1{+}\pi\alpha/\rho)$	—
$\Delta m/m_e$	$\binom{7}{3}\pi^2\alpha$	$\times(1{+}\frac{(n-d)\alpha}{\rho})$	$\times(1{+}\frac{(n-1)\alpha^2}{n+2})$	$-\alpha^2$

Table 2: The correction taxonomy applied to all six BSM observables.

7 Mass Predictions

7.1 The Proton–Electron Mass Ratio

The proton is a ternary (3-node) defect with structural parameter n:

$$\boxed{\frac{m_p}{m_e} = \mu\big(1+2(2n{+}1)\pi\alpha^3\big) + \left(1+\frac{1}{2n}\right)\pi^2\alpha(1{-}\alpha^2) - \alpha^2} \tag{8}$$

Prediction: 1836.152 673 5 (CODATA: 1836.152 673 426(32), agreement < 0.03 ppb).

7.2 The Muon–Electron Mass Ratio

The muon is a binary (2-node) defect excitation with structural parameter d:

$$\boxed{\frac{m_\mu}{m_e} = \frac{d}{2}\big(\tau + \pi\alpha(1-\alpha^2)\big) + \frac{c_1}{4} + \frac{d}{2}\pi\sigma\alpha^3 - \alpha^2} \tag{9}$$

Prediction: 206.768 282 5 (CODATA: 206.768 282 7(46), agreement 1.1 ppb).

7.3 The Tau Lepton and the Generation Problem

The tau mass emerges from the Koide relation, identified as the transverse fraction of a line defect:

$$\boxed{Q \equiv \frac{m_e + m_\mu + m_\tau}{(\sqrt{m_e} + \sqrt{m_\mu} + \sqrt{m_\tau})^2} = \frac{d-1}{d} + \frac{(d-1)\pi^2\alpha^2}{(n-1)\sigma}} \tag{10}$$

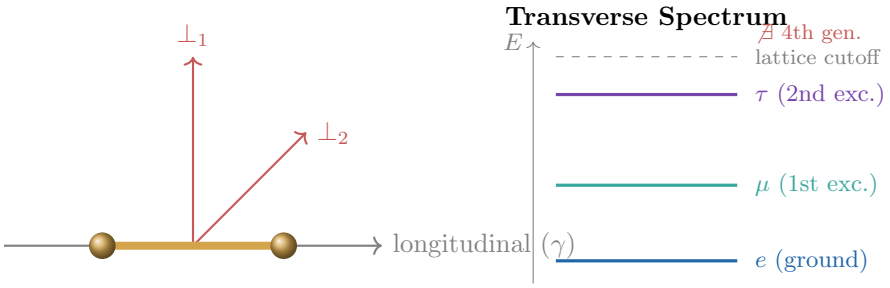

Figure 15: The binary defect and its transverse spectrum. Three bound states (electron, muon, tau) with no fourth generation.

Prediction: $m_\tau/m_e = 3477.4799$ (CODATA: 3477.48 ± 0.57, agreement 0.027 ppm).

7.4 The Higgs Boson Mass

The Higgs is the breathing mode. Of $\sigma = 136$ pairwise scalar modes, $d = 3$ become Goldstone bosons, leaving $\sigma - d = 133$:

$$\boxed{\frac{m_H}{m_p} = (\sigma - d)\left(1 + \frac{\pi\alpha}{\rho}\right) = 133 \times 1.002547 = 133.339} \tag{11}$$

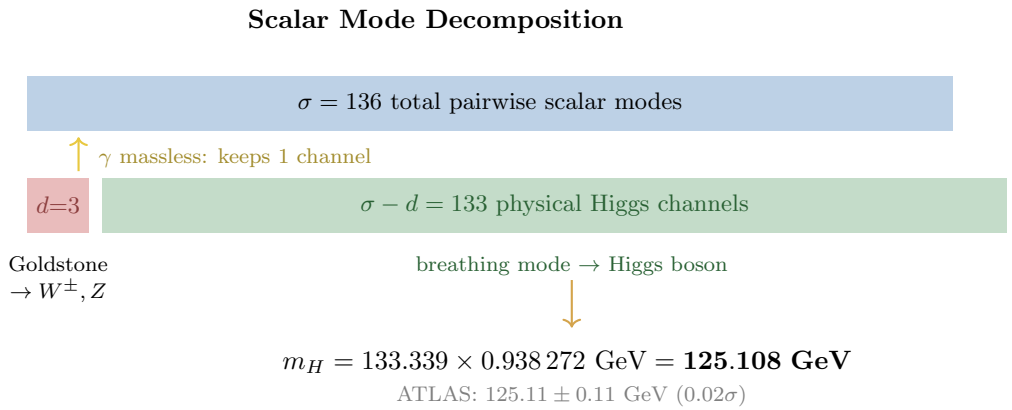

Figure 16: Higgs mass from scalar mode decomposition. The photon's masslessness means $d = 3$ (not $d + 1 = 4$) modes are eaten, raising the Higgs mass by one dressed proton mass.

7.5 The Neutron–Proton Mass Difference

$$\boxed{\frac{\Delta m}{m_e} = \binom{n-1}{d}\pi^2\alpha\left(1 + \frac{(n-d)\alpha}{\rho} - \alpha^2\right) \times \left(1 + \frac{(n-1)\alpha^2}{n+2}\right)} \tag{12}$$

Prediction: $2.531\,029\,91\,m_e$ (Experiment: $2.531\,030\,00(3)\,m_e$, agreement 0.036 ppm).

8 The VP Catalog and Self-Consistency Loop

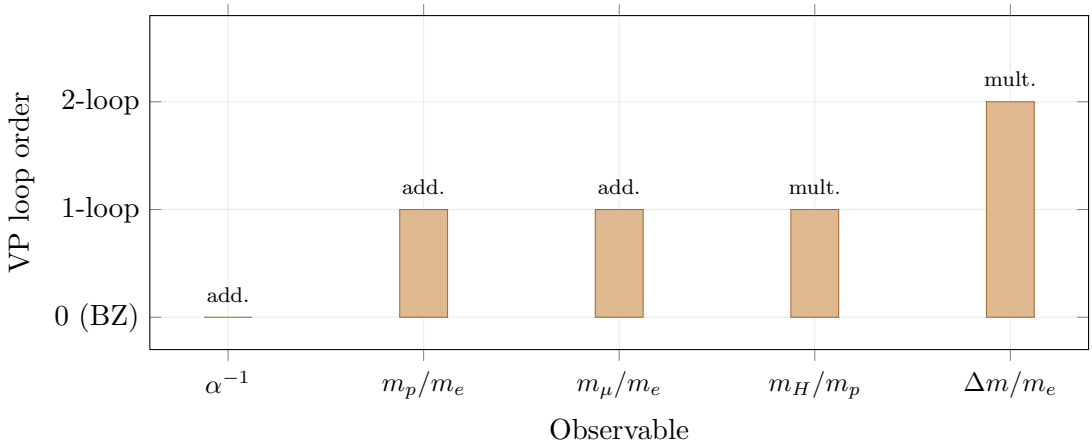

Figure 17: VP loop-order hierarchy. Each VP lives one loop above its tree level.

The photon participates in a closed self-consistency loop:

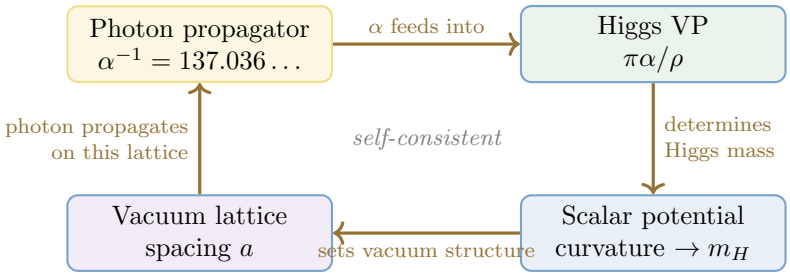

Figure 18: The photon self-consistency loop. The same α that emerges from the Dyson equation enters the Higgs VP and produces a scalar potential whose curvature yields the lattice on which α is defined.

9 Complete Scorecard

Constant	BSM Prediction	Experiment	Agreement	Origin
α^{-1}	137.035 999 177	137.035 999 177(21)	< 0.001 ppb	photon propagator
m_p/m_e	1836.152 673 5	1836.152 673 426(32)	< 0.03 ppb	ternary defect (n)
m_μ/m_e	206.768 282 5	206.768 282 7(46)	1.1 ppb	binary defect (d)
m_τ/m_e	3477.4799	3477.48 ± 0.57	0.027 ppm	Koide (transverse)
m_H/m_p	133.339	133.34(12)	0.02σ	breathing mode
$\Delta m/m_e$	2.531 029 91	2.531 030 00(3)	0.036 ppm	ternary orient.

Table 3: Six fundamental constants from two inputs ($n = 8$, π) plus $d = 3$. Zero free parameters.

10 Structural Architecture

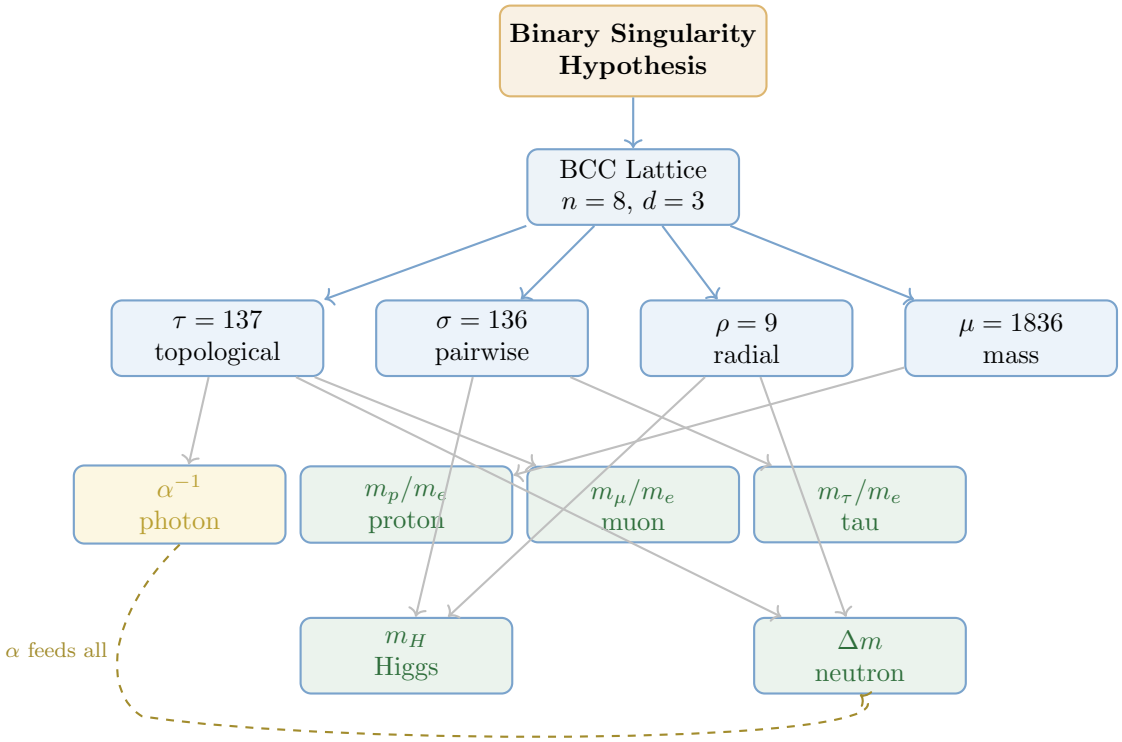

Figure 19: The BSM architectural flow. The photon's α (yellow, highlighted) self-consistently feeds into all other predictions.

11 Falsifiability and Predictions

Higgs Mass Prediction — Falsifiable at the HL-LHC

If HL-LHC converges to	BSM deviation	Status
125.11 GeV (ATLAS)	0.1σ	**Confirmed**
125.20 GeV (world avg.)	4.4σ	**Strongly disfavored**
125.35 GeV (CMS)	11.5σ	**Ruled out**

Structural predictions subject to computational verification:

1. The transverse Laplacian $D_\perp^2$ on the binary defect has exactly 3 bound states (3 lepton generations from geometry).
2. Lattice perturbation theory at one loop on BCC with $g^2 = 1/2$, $N_D = 4$ reproduces $c_1/\tau = \pi^2/(2 \times 137)$.
3. The scalar effective potential on BCC yields tree-level gap $\sigma - d = 133$.
4. Vacuum dispersion is quadratic ($\propto E^2$), undetectable for $a \lesssim \ell_P$.

12 Photon Summary

Property	**BSM lattice account**
Identity	Longitudinal propagation mode of the binary defect; U(1) gauge mode on bonds
Coupling	α = dressed photon propagator (Dyson equation, < 0.001 ppb)
Masslessness	Gauge invariance: flat direction of lattice action along bond
Polarization	$d - 1 = 2$ transverse fluctuations of the bond
Speed of light	Lattice propagation velocity $c = \lim_{k\to 0} \omega/k$
Dispersion	$\omega = (2c/a)\lvert\sin(ka/2)\rvert$; linear for $\lambda \gg a$, deviates near $\lambda \sim a$
Statistics	Bose: $\mathbb{Z}_2$-symmetric mode of the two-node defect
Refraction	Forward scattering off lattice defects (matter) with amplitude $\sim \alpha$
Higgs coupling	Photon propagates on breathing lattice; coupling $= \pi\alpha/\rho$
Scale constraint	Observation requires $a \lesssim \ell_P$ (sub-Planckian)

Table 4: Complete photon characterization in the BSM framework.

13 Open Problems

(a) **First-principles derivation.** Derive all six formulas from the BCC lattice Lagrangian.

(b) **Photon self-energy.** Compute the one-loop $\Sigma(p)$ on BCC with $g^2 = 1/2$, $N_D = 4$ and verify $c_1/\tau = \pi^2/(2 \times 137)$.

(c) **BCC dispersion.** The exact photon dispersion on BCC (direction-dependent velocities, multiple branches) has not been computed from the Dirac operator.

(d) **Absolute energy scale.** The framework predicts dimensionless ratios but not the Higgs vev $v = 246$ GeV or any absolute mass in GeV.

(e) $H \to \gamma\gamma$ **coupling.** The Higgs–photon–photon vertex exists through the breathing-mode modulation with coupling $\sim \alpha/(\sigma - d)$, but an explicit branching ratio has not been derived.

(f) **Electroweak sector.** The Goldstone subtraction connects to $W^{\pm}$, Z but does not yet predict the Weinberg angle or gauge boson mass ratios.

(g) **Graviton.** If the photon is the U(1) mode on bonds, is there a spin-2 mode on plaquettes or higher simplices identifiable with the graviton?

(h) **Quark sector and gravity.** Can the defect classification extend to quarks and the sub-Planckian origin connect to quantum gravity?

"Two sub-Planckian singularities in orbit. A lattice with eight neighbors.
Six constants from two inputs and a transcendental.
The photon is the most precisely predicted object in the framework—
and the object whose question started it all."